International Journal of Energy and Environmental Engineering (2018) 9:169–185
https://doi.org/10.1007/s40095-018-0260-1

ORIGINAL RESEARCH

Adsorption characterization and CO_2 breakthrough of MWCNT/Mg-MOF-74 and MWCNT/MIL-100(Fe) composites

Rached Ben-Mansour[1] · Naef A. A. Qasem[1] · Mohamed A. Habib[1]

Received: 31 October 2017 / Accepted: 6 January 2018 / Published online: 23 January 2018

Abstract

Carbon capture using adsorption processes can significantly mitigate global warming. Mg-MOF-74 is a distinct reticular material amongst other adsorbents owing to its distinguished carbon dioxide adsorption capacity and selectivity under low-pressure applications, while MIL-100(Fe) has lower CO_2 adsorption capacity, but extraordinary thermal and hydrostability in comparison to many classes of MOFs. In this paper, we present CO_2 adsorption characteristics of new compounds formed by the incorporation of multi-walled carbon nanotubes (MWCNTs) into Mg-MOF-74 and MIL-100(Fe). This was done to improve the thermal diffusion properties of the base MOFs to enhance their adsorption capacities. The new composites have been characterized for degree of crystallinity, and the CO_2 and N_2 equilibrium uptake. The real adsorption separation has been investigated by dynamic breakthrough tests at 297 K and 101.325. The equilibrium isotherm results showed that Mg-MOF-74 and 0.25 wt% MWCNT/MIL-100(Fe) (MMC2) have the highest CO_2 uptake in comparison to the other investigated composites. However, the interesting results obtained from breakthrough tests demonstrate that good improvements in the CO_2 adsorption uptake and breakthrough breakpoint over pristine Mg-MOF-74 have been accomplished by adding 1.5 wt% MWCNT to Mg-MOF-74. The improvements of CO_2 adsorption capacity and breakpoint were about 7.35 and 8.03%, respectively. Similarly, the CO_2 adsorption uptake and breakthrough breakpoint over pristine MIL-100(Fe) are obtained by 0.1 wt% MWCNT/MIL-100(Fe) (MMC1) with improvements of 12.02 and 9.21%, respectively.

Keywords Adsorption · Mg-MOF-74 · MIL-100(Fe) · MWCNTs · Characterization · Breakthrough · Carbon capture

Abbreviations

MFC1	0.1 wt% MWCNT/Mg-MOF-74
MFC2	0.25 wt% MWCNT/Mg-MOF-74
MFC3	0.5 wt% MWCNT/Mg-MOF-74
MFC4	0.75 wt% MWCNT/Mg-MOF-74
MFC5	1.5 wt% MWCNT/Mg-MOF-74
MMC1	0.1 wt% MWCNT/MIL-100(Fe)
MMC2	0.25 wt% MWCNT/MIL-100(Fe)
MMC3	0.5 wt% MWCNT/MIL-100(Fe)
MWCNT	Multi-walled carbon nanotubes

List of symbols

C	Concentration (mol/m^3)
D	Diffusion coefficient (m^2/s)
ε	Porosity
k	Adsorption time constant (1/s)
K	Breakthrough fitting constant
K_{eq}	Toth adsorption constant (1/kPa)
L	Adsorbent bed length (m)
n	Toth adsorption constant
q	Adsorption uptake (mmol/g)
Q	Outlet volumetric flow rate (m^3/s^{-1})
Q_F	Feed volumetric flow rate (m^3/s^{-1})
P	Pressure (Pa)
r	Adsorbent particle radius (m)
R	Universal gas constant (J/mol K)
v	Velocity (m/s)
t	Time (s)

Subscripts

CO_2, N_2	Carbon dioxide, nitrogen gas
i	Gas species index
g	Gas
m	Maximum, limited
0, in	Inlet
out	Outlet

✉ Mohamed A. Habib
mahabib@kfupm.edu.sa

[1] Mechanical Engineering Department and KACST-TIC on CCS, King Fahd University of Petroleum and Minerals, Dhahran 31261, Saudi Arabia

Introduction

The fossil fuel burning processes produce greenhouse gases, including CO_2, N_2, and CH_4. Global warming caused by these gases leads apparently to shore floods, hot atmosphere, soil droughts, and damage of eco system. In this scenario, carbon dioxide holds the most significant portion of the flue gases released to the atmosphere [1]. Thus, extensive efforts have been made by scientists, institutions, countries, and environmental organizations to reduce the CO_2 emissions. The principal source of CO_2 is a combustion processes that used fossil fuel. However, the utilization of fossil fuel is still very for satisfying energy demands. Hence, the feasible solution to continue using fossil fuel with mitigation of climate change is Carbon Capture and Storage (CSS).

A massive number of researchers have already studied CO_2 capture using both experimental and simulation approaches as well as synthesizing novel adsorbents [2]. Using adsorption for CO_2 separation is advantageous by the ease of regenerating the adsorbent by being exposed to heat and/or vacuum [3]. The most common known adsorbents are activated carbons and zeolites being exploited for CO_2 separation and storage. Zeolites could adsorb a higher quantity of CO_2 than does by activated carbon at low operating pressures (< 20 kPa) [4, 5], whereas carbon-based adsorbents are better for CO_2 storage applications [5, 6]. Conversely, the obvious merits of carbon adsorbents over zeolites are cost penalties, hydrostability, lower regeneration energy, and easiness of production on a commercial scale [7]. Despite, zeolite-based adsorbents have the relatively higher CO_2 adsorption capacity, especially at lower adsorption pressures (10–30 kPa (abs.) at $T = 30$ °C), the CO_2 uptake is greatly reduced in case of CO_2/H_2O mixture and requires significantly higher heat of regeneration [8, 9].

Since 20 years ago, a novel class of reticulate adsorbents has been discovered and called metal organic frameworks (MOFs) [10, 11]. In this context, the highest adsorption CO_2 adsorption capacity (1470 mg g^{-1}) was reported for MOF-177 at 35 bar [12]. Over time, a large number of MOFs have been developed by scientists for maximize the CO_2 uptake and selectivity.

A certain class of MOFs incorporating functionalized and open metal sites has shown high separation efficiency at ambient conditions like HKUST-1, Mg-MOF-74, and NH_2MIL-53 (Al) [13]. With regard to maximum CO_2 adsorption capacity uptake, a few MOFs have shown a reasonably high CO_2 uptake, such as CPM-5, MIL-53 (Al), UMCM-150, and Ni-STA-12, while others have been evaluated for comparatively lower uptakes like MOF-5 and MOF-177 [13]. A nickel-based MOF, Ni/DOBDC, was also investigated for CO_2 capture and was measured to exhibit a fairly high adsorption capacity [14]. A nickel isonicotinate-based ultramicroporous MOF, 1 [Ni-(4PyC)2·DMF], showed lower parasitic energy than Mg-MOF-74 and good stability with humidity [15].

MOF-74 is the most currently available MOFs with high CO_2 adsorption uptake as well as an excellent CO_2 over N_2 selectivity [16, 17]. More specifically, Mg-MOF-74 was quantitatively identified as the highest adsorbent adsorbs CO_2 at low-pressure conditions (350 mg/g at 298 K) [17]. It is also reported that Mg-MOF-74 showed higher H_2O hydrophilicity (593 ml/g at 298 K) than zeolite [18]. Despite the high CO_2 uptake of Mg-MOF-74, the existence of H_2O reduced the CO_2 capture capacity, unlike HKUST-1, MIL-101(Cr), and MIL-100 (Fe) types [19]. The study [19], moreover, showed the reduction of CO_2 adsorption at different conditions. For example, at 1 bar and 298 K, the CO_2 adsorption capacity of the dry Mg-MOF-74 was about 8.4 mmol/g of CO_2, while with hydration 6.5 and 13%, the CO_2 adsorption capacity values were 6.7 mmol/g and 5.4 mmol/g, respectively [19]. MIL-100(Fe) is remarked as the hydro- and thermal-stable adsorbent. It showed that some increase in CO_2 uptake recorded with increasing RH, (up to 105 mg g^{-1} for CO_2 at 40% RH), with a large decrease in adsorption heat [20].

Less than 2 decades, carbon nanotubes (CNTs) have confirmed a capability towards CO_2 separation [21–25]. Specifically, the functionalized CNTs by amine-groups showed a significant improvement in the CO_2 uptake [26–29]. The CO_2 uptake was reported around 2.59 mmol/g at 293 K using APTES functionalized CNTs. Incorporating CNTs with adsorbents could considerably improve the thermal diffusion of the adsorbents, thereby enhancing the CO_2 adsorption uptake [30–32]. For example, the compound of CNT@13X/$CaCl_2$ exhibited higher thermal conductivity and then more CO_2 uptake than did by 13X/$CaCl_2$ and pristine 13X [30, 31]. Furthermore, the thermal stability along with the adsorption uptake was improved by adding CNT to MIL-101-68 (Al) [32]. Incorporating CNT and lithium ions with MOF $Cu_3(btc)_2$ resulted in improving the CO_2 capacity by about 305% compared with those of the base adsorbent ($Cu_3(btc)_2$) [33]. In addition, the adsorption capacity of CO_2 at high pressure and room temperature (10 bars and 298 K) was improved by adding MWCNT to MIL101 [34].

A considerable number of experimental and numerical research attempts based on CO_2 capture and separation have been conducted so far in terms of breakthrough and pressure and temperature swing adsorption [35–49]. Nevertheless, the majority amount of research chemically concentrated on development of novel adsorbent materials targeted for acquiring high CO_2 adsorption and selectivity. At this point, the poor thermal conductivity shown by a vast majority of these adsorbents has been experienced as a major barrier

in improving the CO_2 uptake of these materials in real applications. In addition, a very limited number of research attempts have conducted the enhancement of CO_2 capture and storage via improving the thermal properties of the base adsorbent. For this reason, this paper aims at investigating the effects of incorporating multi-walled carbon nanotubes (MWCNTs) with Mg-MOF-74 and MIL-100(Fe), with the aim of enhancing the thermal properties of the adsorbents, and investigating the influence of the MWCNT addition on the CO_2 adsorption capacity and breakpoint of the resulting MWCNT/Mg-MOF-74 and MWCNT/MIL-100(Fe) composites. The synthesized and activated Mg-MOF-74 and MIL-100(Fe) have been physically incorporated with different percentages of MWCNTs. They are characterized for the degree of crystallinity, CO_2 adsorption isotherms, and CO_2 adsorption breakthrough. Moreover, the dynamic separations of breakthrough tests are carried out to address the actual CO_2 separation from CO_2/N_2 (20% v/v. CO_2 and 80% v/v. N_2 for MWCNT/Mg-MOF-74, and 15% v/v. CO_2 and 85% v/v. N_2 for MWCNT/MIL100(Fe)) mixture and then computing the level of enhancements on CO_2 uptake and separation.

Experimental work methodology

MWCNT/Mg-MOF-74 and MWCNT/MIL-100(Fe) samples preparation

We have followed a successful procedure for synthesizing Mg-MOF-74 as described in [50]. Briefly, 0.337 g 2,5-dihydroxyterephthalic acid and 1.4 g Mg(NO3)2·6H2O were dissolved in a solution of 135 ml dimethylformamide, 9 ml ethanol, and 9 ml water with sonication for 10 min. The resulting stock solution was decanted into twelve 50 ml bottles. The bottles were tightly capped and heated at 398 K for 26 h. The mother liquor was, then, decanted. Following this, the products were washed with methanol, and then, left immersed in methanol. The products were combined to one bottle and exchanged into fresh methanol daily for 4 days. The activation process was carried out by evacuating the product to dryness and then heated under vacuum at 523 K for 6 h.

The synthesis of MIL-100(Fe) was performed in accordance with a previously reported procedure [51]. We first dissolved $Fe(NO_3)_3{\cdot}9H_2O$ (4.04 g, 0.01 mol) in de-ionized water (50.2 ml, 2.8 mol) and the mixture was completely put in a 125 ml Teflon-liner containing BTC (1.4097 g, 0.00671 mol). After that, the Teflon-liner was tightly sealed inside a stainless steel autoclave and was kept at 383 K for 14 h. After heating, the autoclave was slowly cooled to ambient temperature, after which the "as-synthesized" dark orange solid was recovered using a centrifuge that was operated at 8000 rpm for about 45 min. The as-synthesized MIL-100(Fe) was washed with copious amounts of water and ethanol and finally with an aqueous NH_4F solution in purpose removing any unreacted species. Specifically, the dried solid was, first, immersed in deionized water (60 ml per 1 g of solid) and the resulting suspension was stirred at 70 °C for 5 h. Again, the suspension was centrifuged and the wash process was repeated using ethanol (60 ml) at 65 °C for 3 h. This two-step purification was repeated until the decanted solvent following centrifugation became completely colorless, after which the solid was immersed in a 700 ml aqueous NH_4F solution and stirred at 70 °C for 5 h. The suspension was again centrifuged and the solid was washed 5 times DI water at 60 °C, and finally dried in air at 75 °C for 2 days followed by 95 °C for 2 days.

The MWCNT/Mg-MOF-74 sample designations were based according to the weight percentage of powder form of MWCNTs which was physically mixed with as-synthesis powder form of Mg-MOF-74 as follows. Mg-MOF-74, 0.1 wt% MWCNT/Mg-MOF-74, 0.25 wt% MWCNT/Mg-MOF-74, 0.5 wt% MWCNT/Mg-MOF-74, 0.75 wt% MWCNT/Mg-MOF-74, 1 wt% MWCNT/Mg-MOF-74, and 1.5 wt% MWCNT/Mg-MOF-74 and shortly named as Mg-MOF-74, MFC1, MFC2, MFC3, MFC4, MFC5, and MFC6, respectively. The incorporation of powder form of MWCNT with as-synthesis powder form of MIL-100(Fe) has produced MIL-100(Fe), 0.1 wt% MWCNT/MIL-100(Fe), 0.25 wt% MWCNT/MIL-100(Fe), and 0.5 wt% MWCNT/MIL-100(Fe) which were named as MIL-100(Fe), MMC1, MMC2, and MMC3, respectively. The particle size distribution for selective composites has been conducted using Particles-Size Analyzer, Model S3500, Microtrac, USA.

Powder X-ray diffraction (PXRD) analysis

To determine the crystallinity of composites, PXRD patterns of MWCNT/Mg-MOF-74 were collected using a Bruker D8-Advance (Cu K_α $\lambda = 1.54056$ Å). The operating power of the PXRD system was 30 kV/30 mA and the step-counting method (step = 0.02°, time = 3 s) was used to collect data at range $2\theta = 3$–45° and 298 K. For MIL-100(Fe); the diffraction data were collected between 3 and 45° (2θ) with a total scan time of 3 h.

Scanning electron microscopy (SEM)

Scanning electron microscopy (SEM) was carried out using a TESCAN LYRA3 FEG microscope to test structure of Mg-MOF-74, 1.5 wt% MWCNT/Mg-MOF-74, MIL-100(Fe) and 0.5 wt% MWCNT/MIL-100(Fe). SEM samples were prepared by placing a powder form of samples on Al tapes and sputter coated with gold. The images were obtained at voltage of 20 kV.

Gas physisorption measurements

The first step in the physisorption measurements of CO_2 and N_2 is the sample degassing to remove any guest molecules within the pores of each material. Typically, 50–200 mg of each sample was transferred to pre-weighed empty sample cell with a 9 mm diameter. Degassing was conducted at 150 °C under vacuum for about 17 h for MWCNT/MIL-100(Fe) and 220 °C under vacuum during about 5 h for MWCNT/Mg-MOF-74 using an Autosorb degasser (Quantachrome Instruments, Inc.). Nitrogen adsorption isotherms at 77 K were first recorded to estimate the Brunauer–Emmett–Teller (BET)-specific surface area (S_{BET}), average pore radius, and total pore volume. The interesting equilibrium adsorption isotherms for CO_2 at 273, 298, and 313 K, and for N_2 at ambient temperature (298 K) were recorded. The CO_2 heat of adsorption was evaluated using the adsorption isotherms measured at 273 and 313 K in accordance with the Clausius–Clapeyron equation.

Breakthrough experiments of binary gas mixture ($CO_2 + N_2$)

A dynamic CO_2/N_2 breakthrough setup was constructed to separate CO_2 from a CO_2/N_2 mixture (representing a flue gas), Fig. 1. The home-made setup is composed of a bed column with specifications of Inner diameter = 4 mm, outer diameter = 6 mm, and length = 7 cm. The column was filled with the MWCNT/Mg-MOF-74 composite (about 0.26 g), or the MWCNT/MIL-100(Fe) composite (about 0.74 g). The system includes CO_2 and N_2 cylinders, two MFC (calibrated for CO_2 and N_2 flow rates), two check valves, and bypass tube (for calibrating the gases concentration detected by mass spectrometer from the inlet gas compositions). It, moreover, includes two bourdon absolute pressure (manufactured by Baumer, accuracy ± 1.6%), mass spectrometer (to measure the outlet gases composition leaving from the bed), vacuum pump and electric heater jacket (for regeneration purpose), and interconnecting stainless steel fittings and tubes to regulate the flow of carrier gas within the system.

The first step in the operation of breakthrough setup has involved the degassing of the activated MWCNT/MIL-100(Fe) or MWCNT/Mg-MOF-74 composite sample at 423 K under vacuum for 1 day period to remove any guest gases inside the pores of MWCNT/MIL-100(Fe) or MWCNT/Mg-MOF-74 frameworks. The breakthrough experiments were conducted at 297 K and 101.3 kPa. The flowrate of the feed gas, a mixture of 20% CO_2 and 80% N_2 (v/v) for MWCNT/Mg-MOF-74 samples and 15% CO_2 and 85% N_2 (v/v) for MWCNT/MIL-100(Fe) samples, was kept constant at 20 and 10 sccm for MWCNT/Mg-MOF-74 and MIL-MWCNT/100(Fe) composites, respectively. The full breakthrough capacity of CO_2 and N_2 was measured by evaluating the ratio of compositions of the downstream gas and the feed gas. The CO_2 adsorption capacity of the adsorbents is evaluated from the CO_2 molar flowrate inters and leaves the bed using the expression [42]:

$$q_{co_2} = \frac{1}{m}\left[\int_0^t \left(Q_F C_0 - C(t)Q(t)\right)dt - \varepsilon V C_0\right], \quad (1)$$

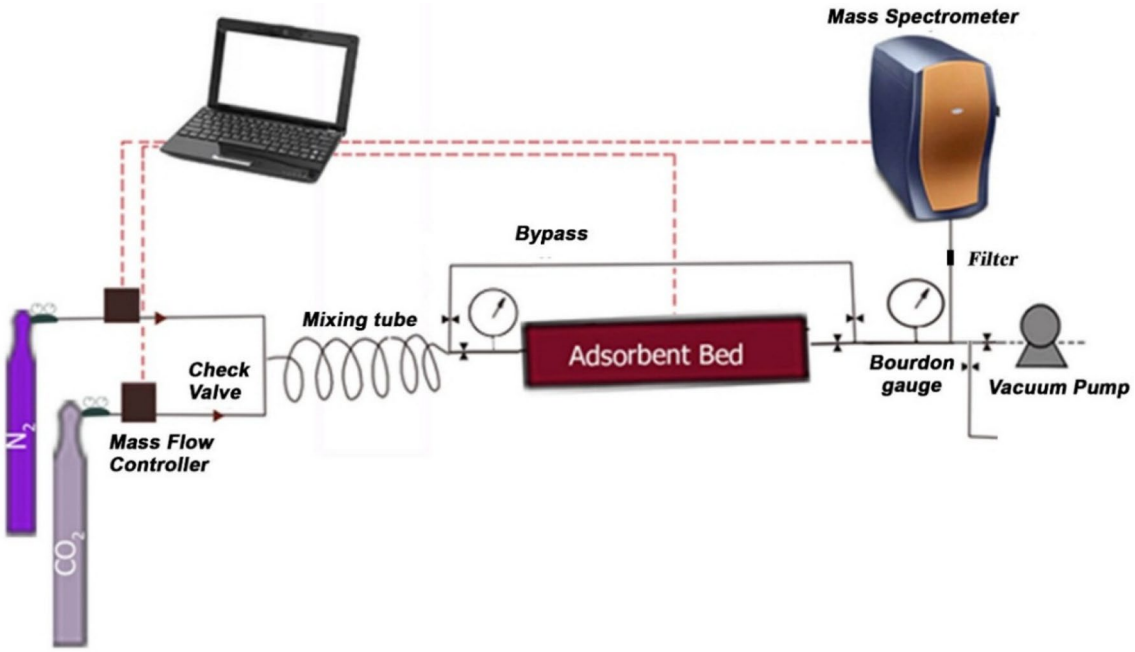

Fig. 1 Scheme of CO_2/N_2 adsorption separation breakthrough setup

where q_{co_2} (mmo/g) represents the CO_2 uptake, Q_F and $Q(t)$ (m^3/s) are the input and output volumetric flow rates, C_0 and $C(t)$ (mol/m^3) are the influent and effluent CO_2 concentrations, t (s) is the time, ε is the bed porosity, and V (m^3) is the bed volume.

The term ($\varepsilon V C_0$) in Eq. 1, which represents the CO_2 amounts still in the bed void (without being adsorbed), has very small values comparing to the other terms, so that, it can be ignored. However, we have considered it in our calculations.

Results and discussion

Powder X-ray diffraction (PXRD) analysis

Figure 2 shows the PXRD patterns of MWCNT/Mg-MOF-74 compounds as well as MIL-100(Fe). It can be seen (Fig. 2a) that the PXRD pattern of MWCNT/Mg-MOF-74 and Mg-MOF-74 samples is in good agreement with the simulated pattern. The incorporation of MWCNTs has not decreased the crystallinity of the framework, as all the intensity peaks locations have represented the Mg-MOF-74 structure. Hence, it can be concluded that the incorporation of less than 1.5 wt% MWCNTs using physical mixing preserves

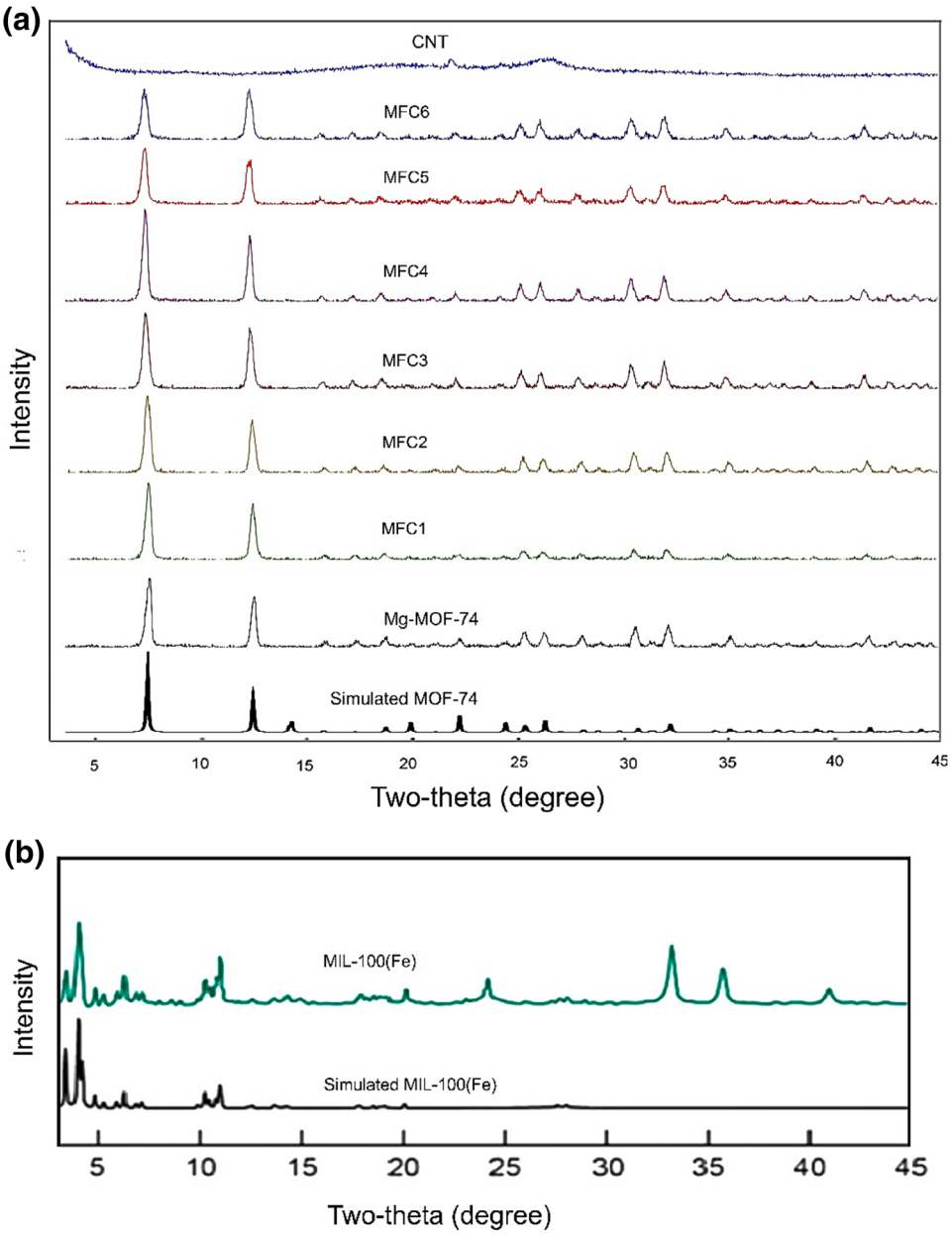

Fig. 2 PXRD patterns for **a** MWCNT/Mg-MOF-74 and **b** MIL-100(Fe)

the characteristic lattice structure of the Mg-MOF-74 framework. The same conclusion was drawn for MWCNT/MIL-100(Fe) as reported in the recent work [51]. Figure 2b is to exhibit that the synthesized MIL-100(Fe) was in good agreement with the simulated pattern.

Electron microscopy analysis

The morphologies of Mg-MOF-74, MIL-100(Fe), 1.5% wt MWCNT/Mg-MOF-74, and 0.5 wt% MWCNT/MIL-100(Fe) composites observed by SEM are shown in Fig. 3. The physical incorporation of MWCNTs does not change the shape of the Mg-MOF-74 and MIL-100(Fe) crystals. The crystal size of Mg-MOF-74 is much bigger than that of MIL-100(Fe).

Adsorption equilibrium isotherms of carbon dioxide and nitrogen

The N_2 equilibrium isotherms for the MWCNT/Mg-MOF-74 and MWCNT/MIL-100(Fe) composites have been measured at 77 K. Table 1 lists the important porosity-related parameters estimated from the N_2 adsorption data MWCNT/Mg-MOF-74 and MWCNT/MIL-100(Fe) composites. The measured BET surface area was almost close to each other in MWCNT/Mg-MOF-74 compounds between 1470 and 1590 m^2/g. In addition, the total pore volume measured at 95% relative pressure (P/P0) and the pore size measured were determined to be almost the same for all the samples by around 0.63–0.71 cc/g and 19 Å, respectively. The Mg-MOF-74 BET surface area and total pore volume values are in good agreement with those reported in the literature [17, 50, 52]. It can be deduced from the data shown in Table 1 that the addition of MWCNTs does not result in substantial

Table 1 Pores characterization of the MWCNT/Mg-MOF-74 and MWCNT/MIL-100(Fe) composites for N_2 at 77 K

Characterizations	S_{BET} (m^2/g)	Pore volume (cc/g)	Average pore radius (Å)
Mg-MOF-74	1518	0.63	8.31
MFC1	1545	0.66	8.55
MFC2	1525	0.65	8.51
MFC3	1579	0.67	8.51
MFC4	1562	0.71	8.51
MFC5	1586	0.69	8.73
MFC6	1477	0.63	8.52
MIL-100(Fe)	1083	0.55	10.07
MMC1	1248	0.61	9.74
MMC2	1464	0.69	9.52
MMC3	1060	0.58	10.94

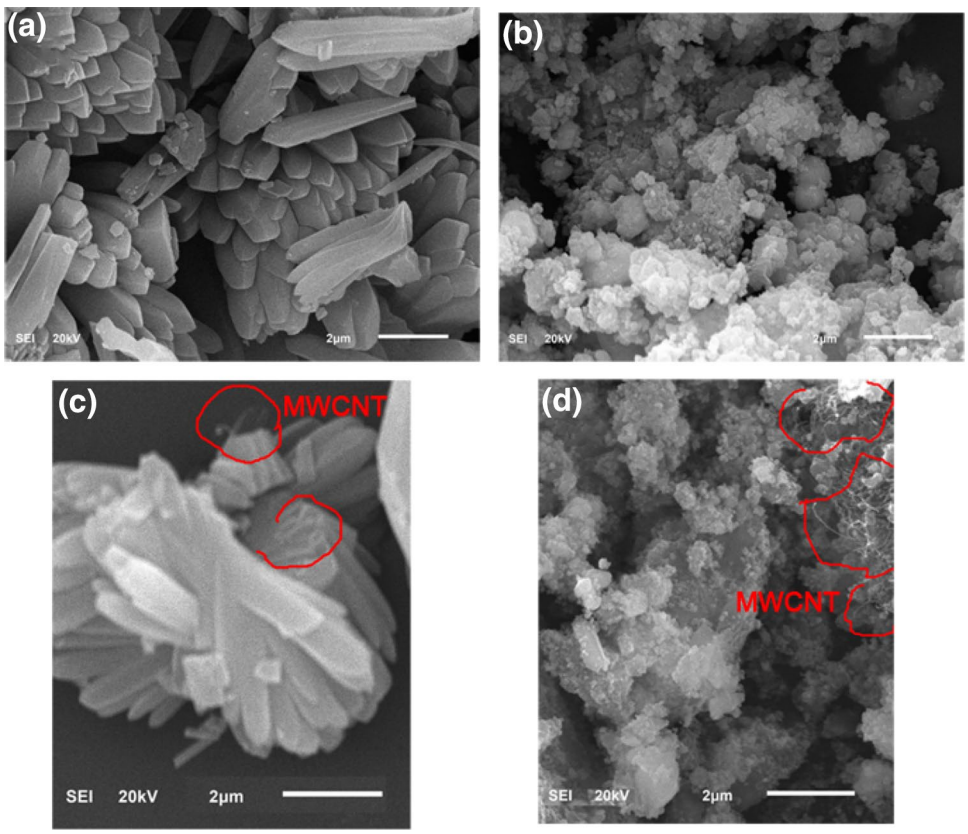

Fig. 3 SEM micrographs of **a** Mg-MOF-74, **b** MIL-100(Fe), **c** 1.5 wt% MWCNT/Mg-MOF-74, and **d** 0.5 wt% MWCNT/MIL-100(Fe)

differences concerning its influence on the porosity-related parameters evaluated for the MWCNT/Mg-MOF-74 compounds. Similarly, the incorporation of MWCNTs with MIL-100(Fe) did not change the porosity-related parameters of pristine MIL-100(Fe). There was almost slight increase in the surface area from 1083 m^2g^{-1} for base MIL-100(Fe) to 1464 m^2g^{-1} for MMC2. The total pore volume at 0.95 relative pressure was around 0.61 and 0.69 cc/g for MMC1 and MMC2, respectively, in comparison to 0.55 cc/g for the pristine MIL-100(Fe). Regarding the pore size, it is clearly that the pore diameter for all the MIL-100(Fe) and composite samples was around 20 Å. These porous-property values are close to those reported for MWCNT/MIL-100(Fe) composites [51]. However, the synthesized MIL-100(Fe) in the present work is not the best qualitative fashion of this adsorbent due to the method of synthesis and purification we have followed. BET and pore volume of MIL-100(Fe) could be varied between 1090 and 2050 m^2g^{-1} (for BET) and from 0.65 to 1.15 cc/g (for average pore volume) [53].

The CO_2 adsorption isotherms for MWCNT/Mg-MOF-74 and MWCNT/MIL-100(Fe) composites, measured at 273, 298, and 313 K, are exhibited in Figs. 4 and 5. It is obvious that the adsorption uptake increased sharply in the region below 15 kPa and increased gradually with increasing adsorption pressure greater than 20 kPa. This behavior gives a good advantage for CO_2 capturing in low-pressure applications including the CO_2 separation from the flue gas (P_{CO2} = 10–20 kPa). However, as expected, an increase in the measured temperature showed an adverse effect on the recorded uptakes for each material. As obvious from Fig. 4, the highest CO_2 uptake has been measured for pristine Mg-MOF-74 followed by MFC1 at all the measured temperatures (273, 298, and 313 K). For MWCNT/MIL-100(Fe) compounds (Fig. 5), the adsorption uptake increased more or less linearly with increasing adsorption pressure. It is obvious that MMC2 showed optimal adsorbed amounts, and MMC1 resulted in the second highest uptake even greater than the pristine MIL-100(Fe) and MMC3 composites, as shown in Fig. 5a–c. It is worth mentioning here that the CO_2 uptake for MWCNT/Mg-MOF-74 composites was much higher than that adsorbed by MWCNT/MIL-100(Fe) compounds. Another point is that the best version of MIL-100(Fe) could adsorb about 1 and 1.52 mmol/g at 0.6 bar for outgassing pretreatments 150 and 250 °C, respectively [54]. Consequently, the reduction of CO_2 capacity of the present MIL-100(Fe) (q = 0.6 mmol/g at 0.6 bar and 298 K) is due to both the followed synthesis method (using $Fe(NO_3)_3{\cdot}9H_2O$) and the activation treatments (75–95 °C).

The N_2 adsorption isotherms for MWCNT/Mg-MOF-74 composites, measured at 298 K, are displayed in Fig. 6a. It is evident that the pristine Mg-MOF-74 exhibited the largest uptake amount, followed by MFC4, MFC1, MFC6, MFC2, MFC5, and MFC3, respectively. Figure 6b shows

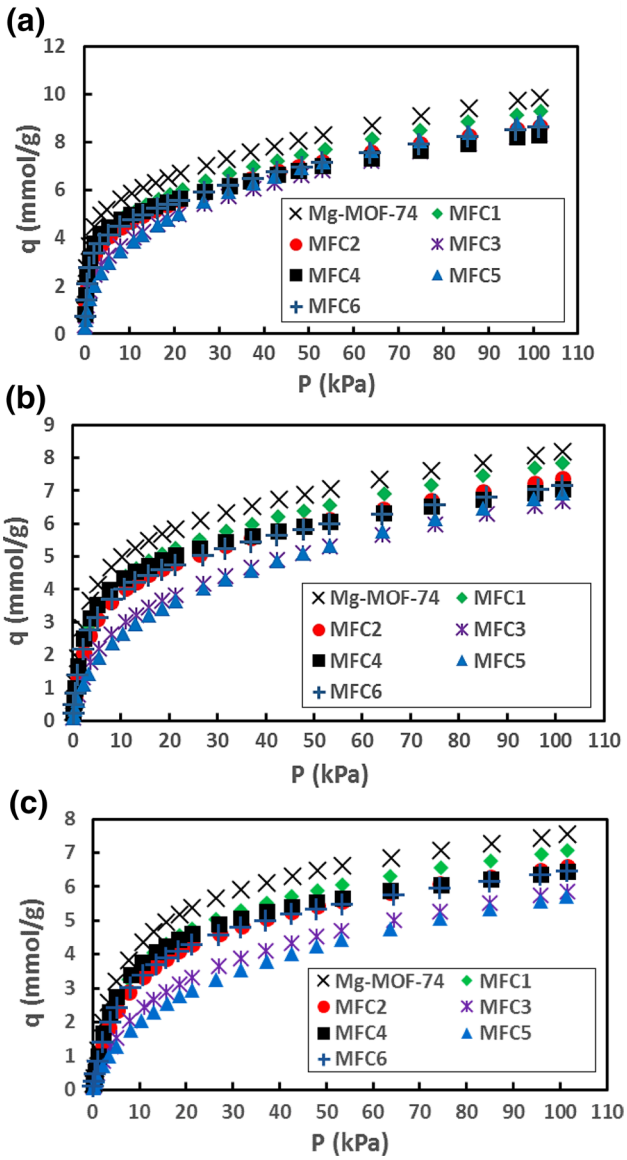

Fig. 4 CO_2 adsorption isotherms of MWCNT/Mg-MOF-74 composites at: **a** 273 K, **b** 298 K, and **c** 313 K

N_2 uptake by MWCNT/MIL-100(Fe) compounds. It is clear that MMC1 had higher adsorbed values in comparison to the other compounds. For both adsorbent composites [MWCNT/Mg-MOF-74 and MWCNT/MIL-100(Fe)], the maximum uptake measured for N_2 was observed to be significantly smaller than that measured earlier for CO_2. In other words, all the samples have been noticed to exhibit preferential selectivity of CO_2 over the N_2.

To represent isotherms in mathematical models, Toth fitting (Eq. 2) is satisfied. For instance, the CO_2 and N_2 values obtained using Toth fitting of MFC6 and MMC1 show an excellent agreement with those of the experimental isotherms as plotted in Fig. 7. The respective fitting parameters at 95% level of confidence are tabulated in Table 2:

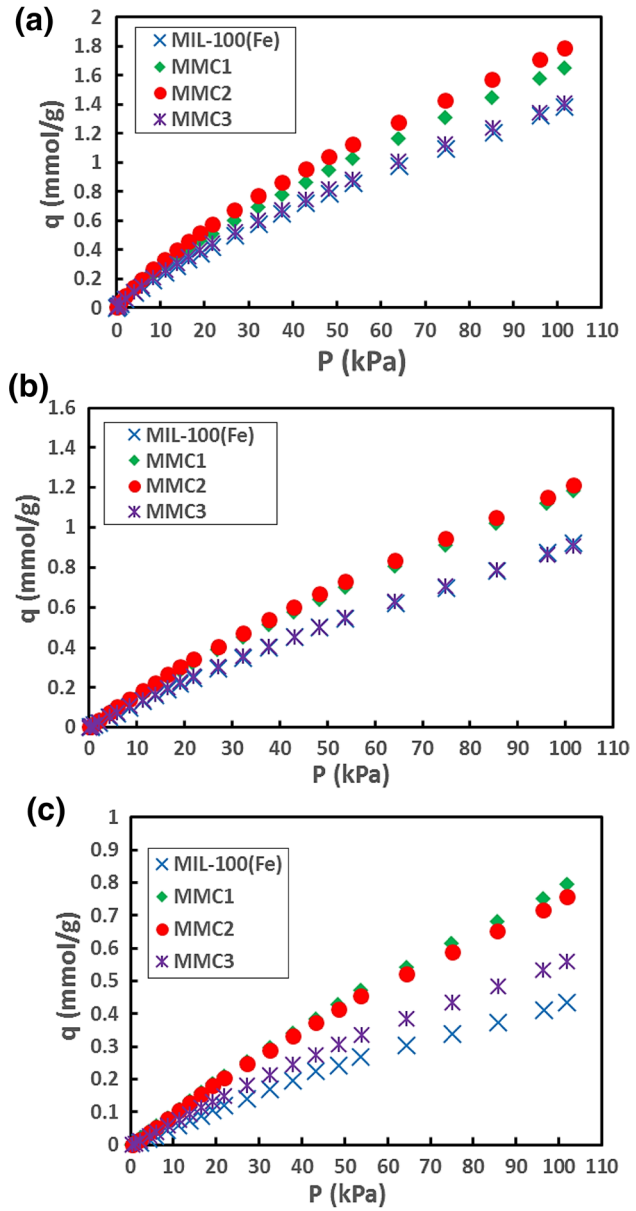

Fig. 5 CO_2 adsorption isotherms of MWCNT/MIL-100(Fe) composites at: **a** 273 K, **b** 298 K, and **c** 313 K

$$q_i = \frac{q_{m,i} K_{\mathrm{eq},i} P_i}{\left[1 + \left(K_{\mathrm{eq},i} P_i\right)^{ni}\right]^{1/ni}}. \quad (2)$$

Here, q is the equilibrium adsorption amount (mmol/g) of species i. q_m, K_{eq}, and n are the Toth fitting constants.

Figure 8a, b depicts the variation of heat of adsorption for CO_2, Q_{st}, against the instantaneous CO_2 uptake for MWCNT/Mg-MOF-74 and MWCNT/MIL-100(Fe) composites. For MWCNT/Mg-MOF-74, the $Q_{\mathrm{st-CO2}}$ values were

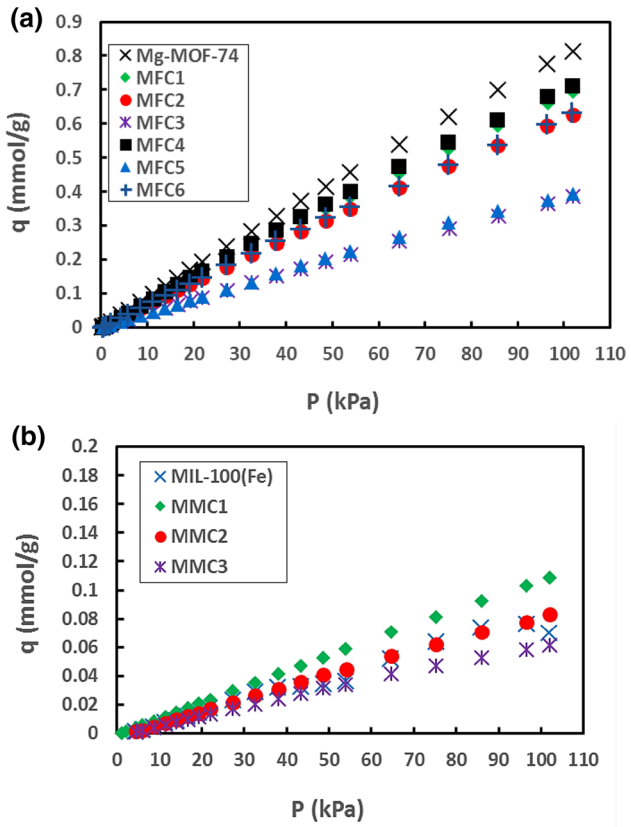

Fig. 6 N_2 adsorption isotherms at 298 K for **a** MWCNT/Mg-MOF-74 and **b** MWCNT/MIL-100(Fe) composites

observed to exhibit a more or less curvilinear correlation with the instantaneous CO_2 uptake, as shown in Fig. 8a. In general, Q_{st-CO2} values locate between 25 and 40 kJ/mol; the high values were sequentially associated with Mg-MOF-74, MFC4, MFC2, and MFC5. In contrast, MFC5 and MCF3 showed lower values of CO_2 adsorption heat. Mg-MOF-74 heat of adsorption profile is close to that reported by Simmons et a. [55].The MWCNT/MIL-100(Fe) composites have been measured to have CO_2 adsorption heat values between 18 and 28 kJ/mol [for $q > 0.3$ mmol/g, Fig. 8b]; the highest values were measured for MIL-100(Fe) about 27.3 kJ/mol (for $q > 0.3$ mmol/g) and the lowest obtained by MMC1 about 18 kJ/mol (for $q > 0.3$ mmol/g). The CO_2 adsorption heat of MIL-100(Fe) show a close values with those of the same adsorbent reported by Mei et al. [56].

Experimental adsorption breakthrough test for MWCNT/Mg-MOF-74 and MWCNT/MIL-100(Fe) composites

Breakthrough experiments have been performed for the binary gas (CO_2/N_2) to quantify the improvements in CO_2 adsorption uptake and breakpoint as a result of the incorporation MWCNTs inside Mg-MOF-74 and MIL-100(Fe). In

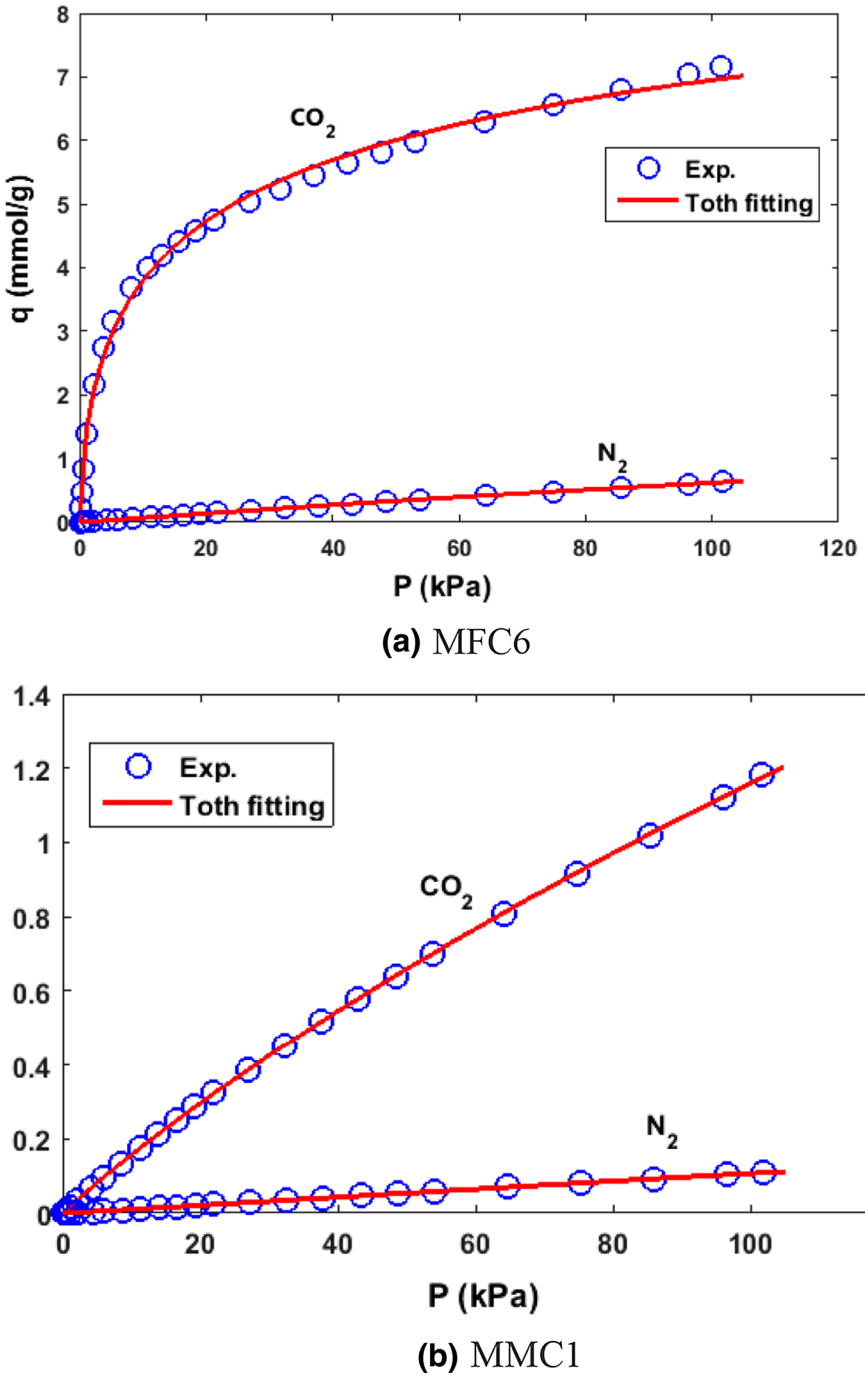

Fig. 7 Equilibrium isotherms and Toth fittings for MFC6 and MMC1 at 298 K. **a** MFC6 and **b** MMC1

a typical procedure, predetermined amounts of MWCNT/Mg-MOF-74 and MWCNT/MIL-100(Fe) composite samples were first transferred to a tube (length $L = 7$ cm, inner diameter $\varnothing = 4$ mm). All breakthrough experiments have been performed at ambient temperature of 297 K.

Particle size used in breakthrough was measured for some selective composites including pure materials and the maximum MWCNTs contents composites, as shown in Fig. 9. Mg-MOF-74 and MFC6 have almost close particle size distribution where the particle size values allocated between 1 and 88 μm. It is also shown that percentage of large sizes have been decreased by adding 1.5 wt% MWCNT. For MWCNT/MIL-100(Fe) particle size distribution, it is obvious from Fig. 9b that the both tested samples (MIL-100(Fe) and MMC3) have similar distribution (between 1 and 1400 μm) with almost the same percentages. This is attributed to the small percentages of MWCNT added to the adsorbents.

For systematic tests, the pressure drop has been diminished to a round zero as monitored by two bourdon meters

Table 2 Toth fitting parameters from experimental CO_2 and N_2 isotherms for MFC6 and MMC1 at 95% level of confidence

Parameter	Estimate	Lower limit	Upper limit
MFC6			
CO_2			
q_m (mmol/g)	12.952	9.843	16.062
$K_{Equation}$ (1/kPa)	0.666	0.266	1.067
n	0.342	0.262	0.423
N_2			
q_m (mmol/g)	2.430	0.979	3.881
$K_{Equation}$ (1/kPa)	0.0029	0.0012	0.0045
n	1.399	0.921	1.876
MMC1			
CO_2			
q_m (mmol/g)	21.628	6.878	36.379
$K_{Equation}$ (1/kPa)	8.42×10^{-4}	3.17×10^{-4}	13.66×10^{-4}
n	0.529	0.425	0.634
N_2			
q_m (mmol/g)	0.157	− 0.040	0.354
$K_{Equation}$ (1/kPa)	69.1×10^{-4}	-17.24×10^{-4}	155.56×10^{-4}
n	6.320	− 9.136	21.776

at the inlet and outlet of the bed. The adsorbent bed was packed with almost the same packing density by about 0.292 ± 0.005 and 0.842 ± 0.002 g/cc for MWCNT/Mg-MOF-74 and MWCNT/MIL-100(Fe) compounds, respectively. The samples have been pre-treated by heating process for 20 h at about 423 K under vacuum. The experimentally measured CO_2 and N_2 adsorption breakthrough curves for MWCNT/Mg-MOF-74 and MWCNT/MIL-100(Fe) composites are displayed in Fig. 10. As evident, the outlet concentration ratios calculated each of these two gases have been plotted against the measurement time. In general, it was observed in all the tested samples that the concentration ratio evaluated for CO_2 at the bed outlet remained constant at zero for some time (e.g., about 6–7 min for MWCNT/Mg-MOF-74 and 2–3 min for MWCNT/MIL-100(Fe) compounds), whereas the concentration ratio for N_2 increased up to about 1.3 (almost molar fraction = 1) owing to the absence of CO_2 which was pre-adsorbed into the Mg-MOF-74 or MIL-100(Fe) composite adsorbent bed. Following the first adsorption minutes of measurement time, the CO_2 concentration ratio was observed to increase up to 1, whereas the concentration ratio of N_2 was evaluated to gradually drop to a value close to 1. For MWCNT/Mg-MOF-74 composites, the optimal value of the breakpoint, a time at which the concentration ratio of the bed outlet has been evaluated to be less than 5%, was measured to be about 8.16 min (28.4 min/g) for MFC6 against 7.5 min (27.67 min/g) for Mg-MOF-74. This was followed by the value measured for MFC4 of about 8.1 min, and then by 7.96 min for MFC1 (Fig. 10a). In the same manner, the highest breakthrough breakpoint obtained by MWCNT\MIL-100(Fe) was associated with MMC2 by about 3.21 min (4.33 min/g) (Fig. 10b). The next breakthrough point was obtained by MMC1 at about 3.19 min (4.32 min/g), and, then, by pristine MIL-100(Fe) at about 2.9 min (3.69 min/g).

Adsorption breakthrough and separation processes can be also investigated numerically as described in our previous works [57–59]. In addition, adsorption breakthrough curves, can be analytically represented by fitting the experimental curves using some approaches reported in the literature; one of these approaches is expressed in the following equation [60, 61],

$$\frac{C\_out}{C\_in} = \frac{1}{2}\mathrm{erfc}\left(\sqrt{\xi} - \sqrt{\tau} - \frac{\sqrt{\xi}}{8} - \frac{\sqrt{\tau}}{8}\right), \tag{3}$$

where

$$\xi = kK\frac{L}{v}\left(\frac{1-\varepsilon}{\varepsilon}\right), \tag{4}$$

$$\tau = k\left(t - \frac{L}{v}\right). \tag{5}$$

Here, k an K are fitting constant; k (1/s), called adsorption time constant, could be used to determine the diffusion coefficient ($k = \frac{15D}{r^2}$, D (m^2/s) is the diffusion coefficient and r (m) is the adsorbent particle radius), L (m) is the bed length, and v (m/s) is the flow velocity. The breakthrough time (t) is taken in seconds.

For example, Fig. 11 shows the analytical and experimental adsorption breakthrough of carbon dioxide adsorbed by MWCNT/Mg-MOF-74 composites. The analytical results using Eq. (3) provide a good indication to the whole adsorption time and behavior that are as close as to those of the experimental curves. The time constant values (k) obtained from analytical curves are 0.258, 0.248, 0.164, 0.392, 0.433, 0.368, and 0.255 1/s for Mg-MOF-74, MFC1, MFC2, MFC3, MFC4, MFC5, and MFC6, respectively.

To evaluate the improvements of CO_2 adsorption capacity and breakpoint by adding MWCNT to Mg-MOF-74 and to MIL-100(Fe), the adsorbed amounts of CO_2 have been calculated from the experimental breakthrough curves

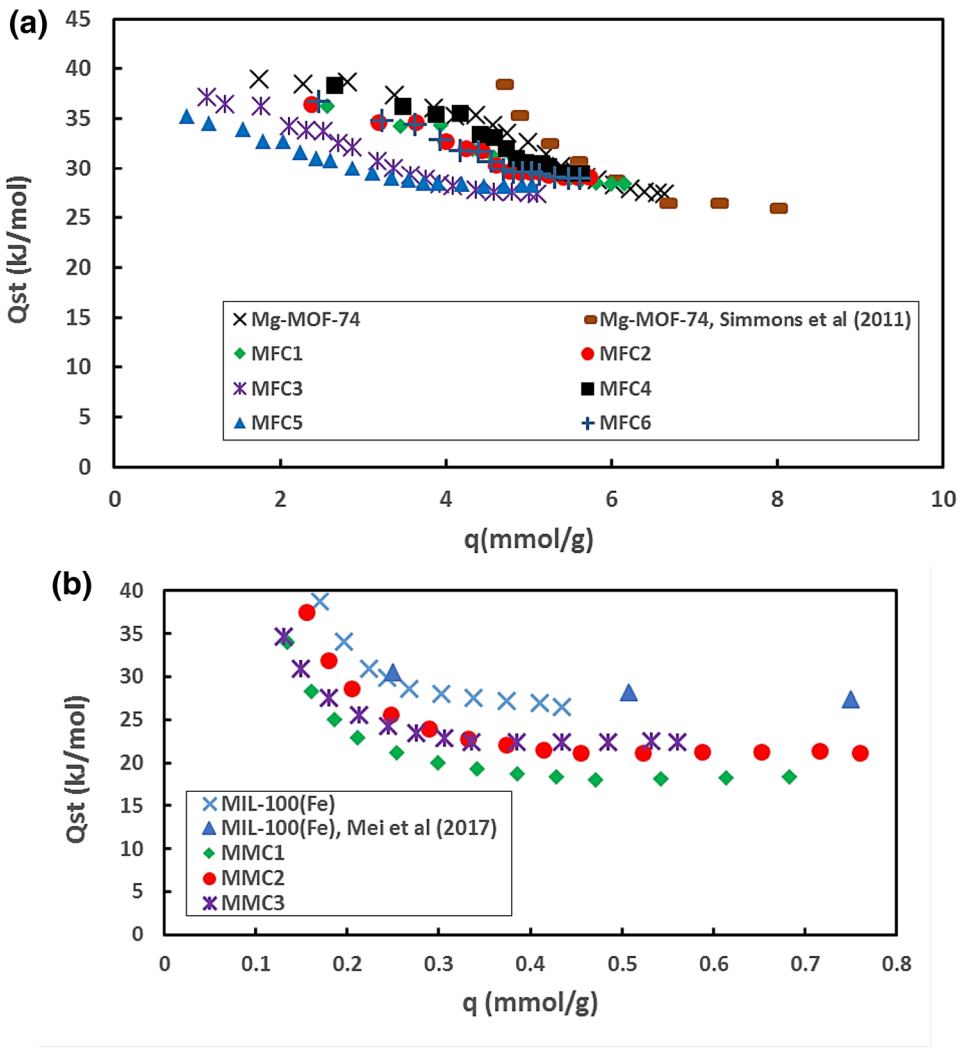

Fig. 8 CO_2 heat of adsorption (Q_{st}) **a** MWCNT/Mg-MOF-74 and **b** MWCNT/MIL-100(Fe) composites

using Eq. 1. The maximum CO_2 adsorption capacity for base Mg-MOF-74 and MIL-100(Fe) calculated from the respective breakthrough curve was estimated to be about 5.46 and 0.37 mmol/g, respectively. The maximum CO_2 uptakes along with the adsorption breakpoint ratios for Mg-MOF-74 as well as each of the six MWCNT/Mg-MOF-74 composites are displayed in Fig. 12a. As evident, each of the six composites, except MFC2 and MFC3, exhibited a good improvement over pristine Mg-MOF-74 with regard to both the adsorption capacity and the adsorption breakpoint ratio values. More specifically, the most optimum combination of adsorption capacity and breakpoint ratio values have been evaluated for MFC6 which has shown an improvement of 7.35 and 8.03% over pristine Mg-MOF-74 for adsorption capacity and breakpoint ratio, respectively. This pair of statistics was followed by MFC1, MFC4, and MFC5 composites for which the corresponding improvements in adsorption capacity and breakpoint values over pristine Mg-MOF-74 have been evaluated to be 4.43 and 5.71, 2.21 and 7.3%, and 1.49 and 4.98%, respectively. It is worth mentioning here that each of the MFC6, MFC1, and MFC4 composites has already been characterized for lower values of heat of adsorption for CO_2 in comparison with pristine Mg-MOF-74, as shown earlier in Fig. 8a. This, theoretically, implies that each of these composites should not only exhibit higher CO_2 uptake values than pristine Mg-MOF-74, but also require comparatively lower energy for regeneration process (recycling recovery).

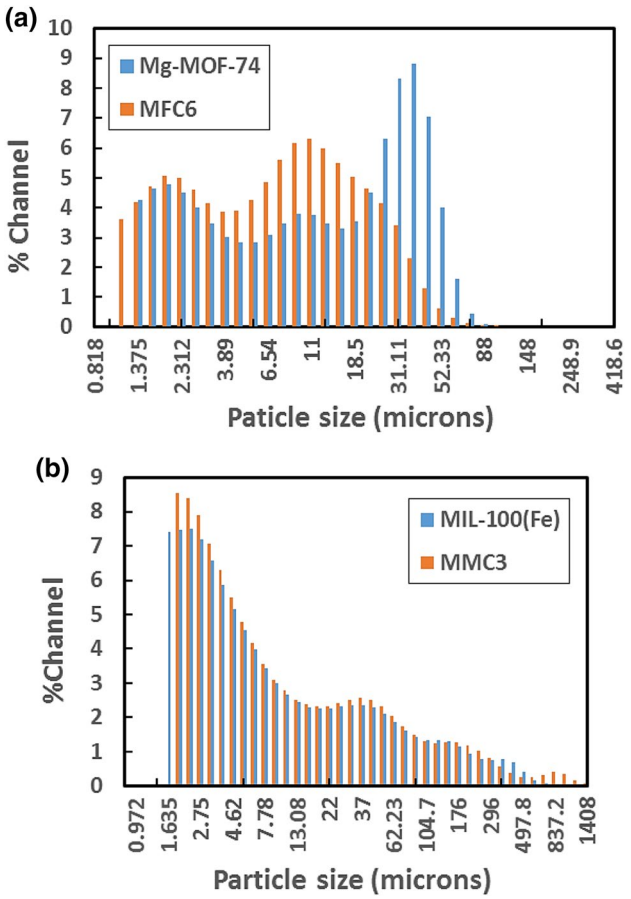

Fig. 9 Particle size distribution (microns) for **a** Mg-MOF-74 and MFC6, and **b** MIL-100(Fe) and MMC3

Figure 12b shows the improvement in both adsorption capacity and breakpoint due to adding MWCNT to the pristine MIL-100(Fe). As evident, MMC1 exhibited an optimal improvement reaches 12.02 and 9.21% for CO_2 adsorption capacity and breakpoint, respectively. This improvement was followed by MMC2 for measured adsorption uptake and breakpoint about 8.74 and 9.47%, respectively, comparing with the base adsorbent (MIL-100(Fe)). On the contrary, the evaluated adsorption uptake and breakpoint improvement values for MFC2, MFC3, and MMC3 showed lower performance than the base adsorbents. This attribute indicates that there is no a uniform improvement can be obtained for the incorporation of CNT with MOFs. The detected improvement in the CO_2 adsorption capacity and breakpoint primarily refers to an improvement in the thermal properties of Mg-MOF-74 and MIL-100(Fe) frameworks upon the incorporation of MWCNTs [30–32]. As the thermal conductivity of CNT is significantly high (2000–5000 W $m^{-1}K^{-1}$) [62], the MWCNT/Mg-MOF-74 and MWCNT/MIL-100(Fe) composites' effective thermal conductivity values could accordingly be higher than those of pristine adsorbents (0.2–0.4 W $m^{-1}K^{-1}$). Therefore, the heat diffusion across the bulk composites is enhanced during adsorption processes, which helps in cooling down the adsorbent and enhances CO_2 adsorption uptake. Furthermore, the enhancement of effective thermal conductivity of adsorbents helps in quickly heating the adsorbent particles during and desorption process which in turns accelerating the CO_2 evacuation from the adsorbent.

This research confirms a comparative dynamic CO_2 uptake compared to the published data shown in Table 3. The MIL-100(Fe) shows the lowest values of adsorption in a comparison to AC, 13X and Mg-MOF-74, while Mg-MOf-74 and MFC6 have the highest CO_2 uptake. Mg-MOF-74 dynamic CO_2 uptake was about 5.46 mmol/g which is greater than 4.06 mmol/g reported in the literature [17, 50], because it was, in this study, measured at 20% CO_2 molar fraction. The cost of adding very low quantity of MWCNT (< 1.5 wt%) to the adsorbents is believed to be neglected in a comparison to the CO_2 separation improvements.

In the literature, chemists usually use the adsorption isotherm data to compare the CO_2 capacities of different adsorbents. However, we found out by carrying both adsorption isotherm measurements and adsorption breakthrough experiments that they can give different ratings of adsorption capacity. Keeping in mind that adsorption isotherm measurements are taken under constant temperatures, while the breakthrough measurements are not, as the breakthrough bed is allowed to vary its temperature due to the heat dissipation from the adsorbent to the ambient or surrounding environments. The improved thermal diffusion cools down the adsorbent quickly. Therefore, the cooler is adsorbent, the higher is CO_2 uptake which is also confirmed in the isotherms. The most accurate adsorption capacity if we are joining to use a PSA/VSA/TSA is that measured in a breakthrough setup.

Conclusions

Two types of MOFs, Mg-MOF-74 and MIL-100(Fe), were synthesized and incorporated with MWCNTs. In total, seven compounds of Mg-MOF-74 materials containing 0, 0.1, 0.25, 0.5, 0.75, 1, and 1.5 wt% MWCNTs and four compounds of MIL-100(Fe) involving 0, 0.1, 0.25, and 0.5 wt%

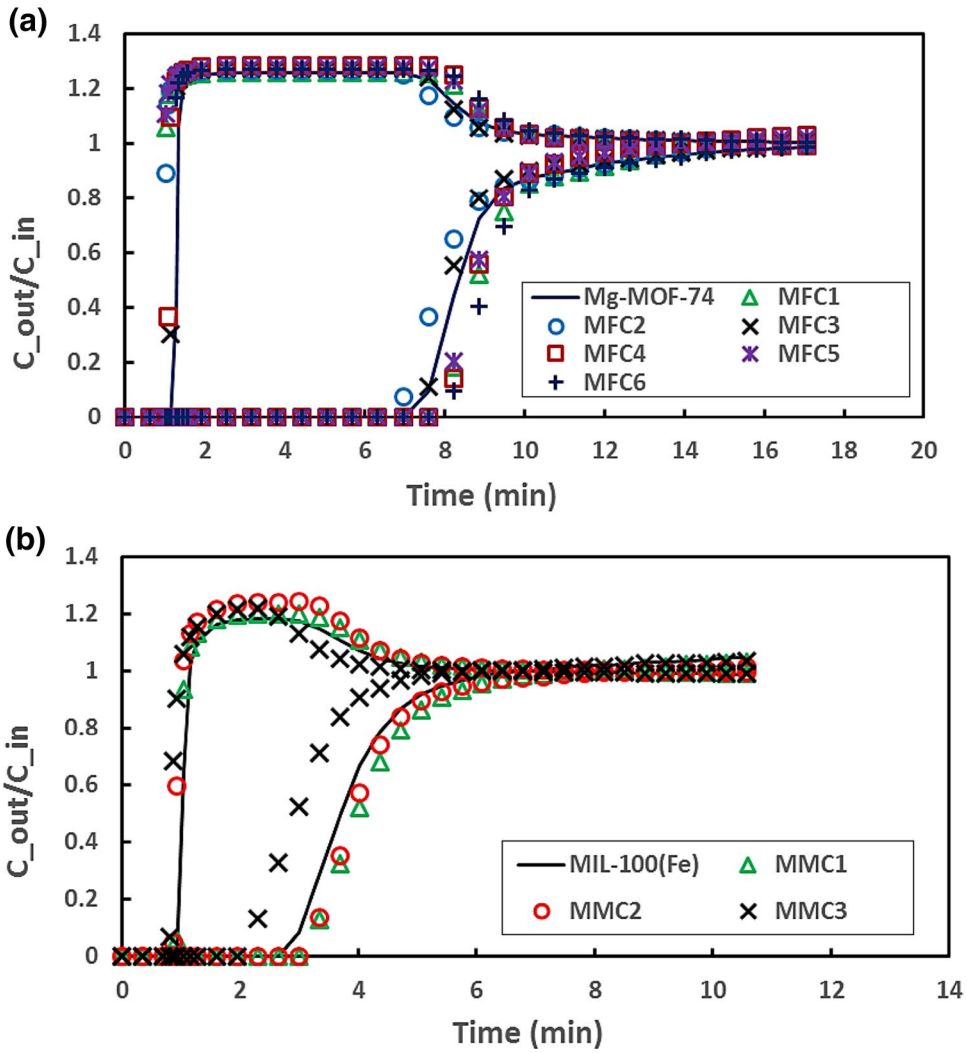

Fig. 10 Breakthrough curves for **a** MWCNT/Mg-MOF-74 composites for CO_2/N_2 (0.2/0.8 v/v) and **b** MWCNT/MIL-100(Fe) composites for CO_2/N_2 (0.15/0.85 v/v), measured at 297 K and 101.3 kPa

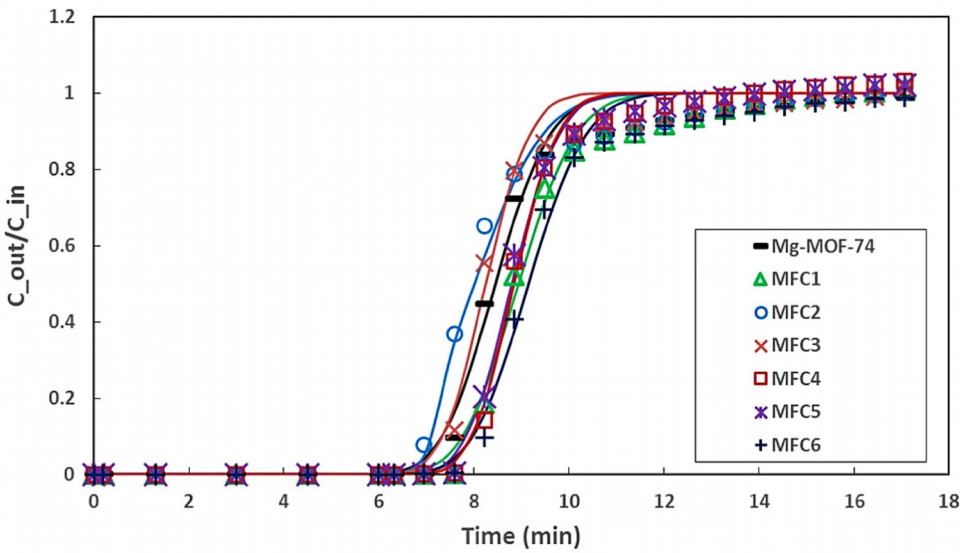

Fig. 11 Analytical representation of CO_2 breakthrough curves of MWCNT/Mg-MOF-74 composites; solid lines are analytical results; symbols are experimental data

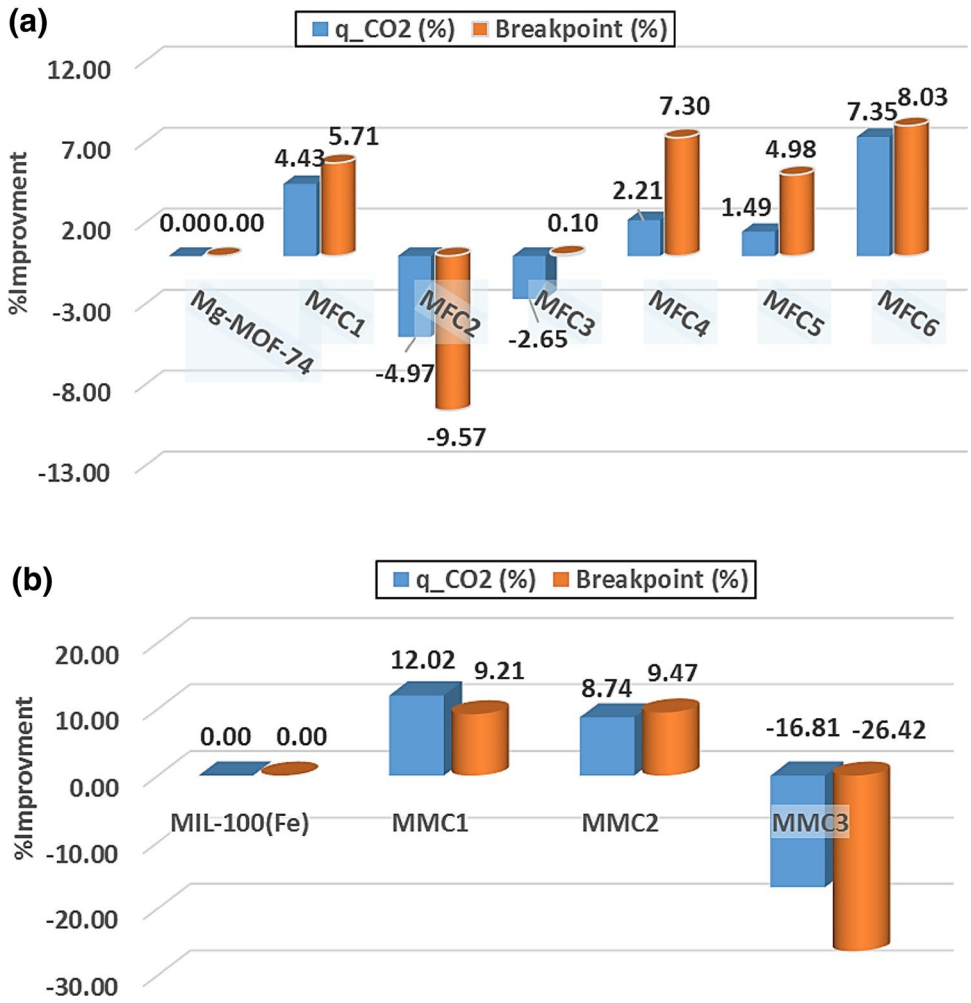

Fig. 12 CO_2 uptake (cubic bars) and adsorption breakpoint (cylindrical bars) enhancements for **a** MWCNT/Mg-MOF-74 and **b** MWCNT/MIL-100(Fe) composites measured at 297 K

Table 3 Dynamic CO_2 uptake of adsorbents

Adsorbent	Temperature (K)	CO_2 vol%	CO_2 capacity (mmol/g)	References
Mg-MOF-74	298	15	4.06	[17, 50]
AC	301	20	0.734	[42]
MIL-101(Cr)	298	10	0.49	[63]
13X	297	20	2.56	[64]
CNT/13X	297	20	3.29	[64]
Mg-MOF-74	297	20	5.46	This work
MFC6	297	20	5.86	This work
MIL-100(Fe)	297	15	0.37	This work
MMC1	297	15	0.41	This work

MWCNT have been characterized for the degree of crystallinity, intrinsic porosity, CO_2 adsorption capacity and separation, and dynamic adsorption breakthrough tests. The powder X-ray diffraction patterns as well as the porosity-related parameters for each of the composites did not include any substantial variation in peak intensities and peak locations, BET surface area, and pore volume and size, indicating that the crystal lattices of Mg-MOF-74 and MIL-100(Fe) were unaffected by the incorporation of MWCNTs using the physical mixing (up to 1.5 wt% MWCNT for Mg-MOF-74 and 0.5 wt% MWCNT for MIL-100(Fe).

Equilibrium adsorption isotherms of CO_2 measured at 273, 298, and 313 K, and N_2 adsorption isotherms measured at 298 K confirm that the highest adsorption capacities for each of these two gases are exhibited by Mg-MOF-74 and 0.25 wt% MWCNT/MIL-100(Fe) (MMC2). Overall, the MWCNT/Mg-MOF-74 composites have much larger adsorption uptake values than those of MWCNT/MIL-100(Fe) composites.

The key performance evaluation of the MWCNT/Mg-MOF-74 and MWCNT/MIL-100(Fe) composites has been achieved through the measurement of actual time-variant CO_2 breakthrough curves, which have revealed a good improvement in CO_2 adsorption capacity as well as adsorption breakpoint due to the incorporation of MWCNTs in the Mg-MOF-74 and MIL-100(Fe) frameworks. The most optimum combination of these characteristics has been observed

for an incorporation of 1.5 wt% MWCNTs in Mg-MOF-74, MFC6, which has adsorption capacity of 5.86 mmol/g with corresponding heat of adsorption about 28.27 kJ/mol against 5.46 mmol/g and 30.02 kJ/mol for pure Mg-MOF-74. The estimated improvements of CO_2 adsorption capacity and breakpoint, obtained from breakthrough using 1.5 wt% MWCNTs/Mg-MOF-74, were about 7.35 and 8.03% over pristine Mg-MOF-74. The incorporation of 0.1 wt% MWCNTs in MIL-100(Fe), MMC1, moreover, improves the adsorption capacity to about 0.414 mmol/g with low corresponding heat of adsorption about 18.34 kJ/mol in comparison to 0.370 mmol/g and 27.20 kJ/mol for MIL-100(Fe). The adsorption uptake and breakpoint enhancements of 0.1 MWCNT/MIL-101(Fe) over pristine MIL-100(Fe) were about 12.02 and 9.21%, respectively.

Acknowledgements The authors thank KACST (CCS-TIC #32-753) at KFUMP for the support received under Project CCS10. The support of Deanship of Research, KFUPM, is also acknowledged.

References

1. D'Alessandro, D.M., McDonald, T.: Toward carbon dioxide capture using nanoporous materials. Pure Appl. Chem. **83**(1), 57–66 (2010)
2. Ben-Mansour, R., Habib, M.A., Bamidele, O.E., Basha, M., Qasem, N.A.A., Peedikakkal, A., Laoui, T., Ali, M.: Carbon capture by physical adsorption: materials, experimental investigations and numerical modeling and simulations—a review. Appl. Energy **161**, 225–255 (2016)
3. Songolzadeh, M., Ravanchi, M.T., Soleimani, M.: Carbon dioxide capture and storage: a general review on adsorbents. World Acad. Sci. Eng. Technol. **70**, 225–232 (2012)
4. Choi, S., Drese, J.H., Jones, C.W.: Adsorbent materials for carbon dioxide capture from large anthropogenic point sources. Chemsuschem **2**(9), 796–854 (2009)
5. Siriwardane, R.V., Shen, M.-S., Fisher, E.P., Poston, J.A.: Adsorption of CO_2 on molecular sieves and activated carbon. Energy Fuels **15**(2), 279–284 (2001)
6. Mazumder, S., van Hemert, P., Busch, A., Wolf, K.H.A.A., Tejera-Cuesta, P.: Flue gas and pure CO_2 sorption properties of coal: a comparative study. Int. J. Coal Geol. **67**(4), 267–279 (2006)
7. Plaza, M.G., González, A.S., Pevida, C., Pis, J.J., Rubiera, F.: Valorisation of spent coffee grounds as CO_2 adsorbents for postcombustion capture applications. Appl. Energy **99**, 272–279 (2012)
8. Chue, K.T., Kim, J.N., Yoo, Y.J., Cho, S.H., Yang, R.T.: Comparison of activated carbon and zeolite 13X for CO_2 recovery from flue gas by pressure swing adsorption. Ind. Eng. Chem. Res. **34**(2), 591–598 (1995)
9. Harlick, P.J.E., Sayari, A.: Applications of pore-expanded mesoporous silicas. 3. Triamine silane grafting for enhanced CO_2 adsorption. Ind. Eng. Chem. Res. **45**(9), 3248–3255 (2006)
10. Li, J.-R., Sculley, J., Zhou, H.-C.: Metal-organic frameworks for separations. Chem. Rev. **112**(2), 869–932 (2012)
11. Nugent, P., Belmabkhout, Y., Burd, S.D., Cairns, A.J., Luebke, R., Forrest, K., Pham, T., Ma, S., Space, B., Wojtas, L., Eddaoudi, M., Zaworotko, M.J.: Porous materials with optimal adsorption thermodynamics and kinetics for CO_2 separation. Nature **495**(7439), 80–84 (2013)
12. Millward, A.R., Yaghi, O.M.: Metal–organic frameworks with exceptionally high capacity for storage of carbon dioxide at room temperature. J. Am. Chem. Soc. **127**(51), 17998–17999 (2005)
13. Sabouni, R., Kazemian, H., Rohani, S.: Carbon dioxide adsorption in microwave-synthesized metal organic framework CPM-5: equilibrium and kinetics study. Microporous Mesoporous Mater. **175**, 85–91 (2013)
14. Wang, H., Qu, Z.G., Zhang, W., Chang, Y.X., He, Y.L.: Experimental and numerical study of CO_2 adsorption on Ni/DOBDC metal–organic framework. Appl. Therm. Eng. **73**(2), 1501–1509 (2014)
15. Nandi, S., Collins, S., Chakraborty, D., Banerjee, D., Thallapally, P.K., Woo, T.K., Vaidhyanathan, R.: Ultralow parasitic energy for postcombustion CO_2 capture realized in a nickel isonicotinate metal–organic framework with excellent moisture stability. J. Am. Chem. Soc. **139**(5), 1734–1737 (2017)
16. Adhikari, A.K., Lin, K.-S.: Improving CO_2 adsorption capacities and CO_2/N_2 separation efficiencies of MOF-74(Ni, Co) by doping palladium-containing activated carbon. Chem. Eng. J. **284**, 1348–1360 (2016)
17. Yang, D.-A., Cho, H.-Y., Kim, J., Yang, S.-T., Ahn, W.-S.: CO_2 capture and conversion using Mg-MOF-74 prepared by a sonochemical method. Energy Environ. Sci. **5**(4), 6465–6473 (2012)
18. Yang, D.-A., Cho, H.-Y., Kim, J., Yang, S.-T., Ahn, W.-S.: CO_2 capture and conversion using Mg-MOF-74 prepared by a sonochemical method. Energy Environ. Sci. **5**(4), 6465–6473 (2012)
19. Yu, J., Balbuena, P.B.: Water effects on postcombustion CO_2 Capture in Mg-MOF-74. J. Phys. Chem. C **117**(7), 3383–3388 (2013)
20. Soubeyrand-Lenoir, E., Vagner, C., Yoon, J.W., Bazin, P., Ragon, F., Hwang, Y.K., Serre, C., Chang, J.-S., Llewellyn, P.L.: How water fosters a remarkable 5-fold increase in low-pressure CO_2 uptake within mesoporous MIL-100(Fe). J. Am. Chem. Soc. **134**(24), 10174–10181 (2012)
21. Cinke, M., Li, J., Bauschlicher, C.W., Ricca, A., Meyyappan, M.: CO_2 adsorption in single-walled carbon nanotubes. Chem. Phys. Lett. **376**(5–6), 761–766 (2003)
22. Hsu, S.-C., Lu, C., Su, F., Zeng, W., Chen, W.: Thermodynamics and regeneration studies of CO_2 adsorption on multiwalled carbon nanotubes. Chem. Eng. Sci. **65**(4), 1354–1361 (2010)
23. Lithoxoos, G.P., Labropoulos, A., Peristeras, L.D., Kanellopoulos, N., Samios, J., Economou, I.G.: Adsorption of N_2, CH_4, CO and CO_2 gases in single walled carbon nanotubes: a combined experimental and Monte Carlo molecular simulation study. J. Supercrit. Fluids **55**(2), 510–523 (2010)
24. Su, F., Lu, C., Cnen, W., Bai, H., Hwang, J.F.: Capture of CO_2 from flue gas via multiwalled carbon nanotubes. Sci. Total Environ. **407**(8), 3017–3023 (2009)
25. Zhou, X., Yi, H., Tang, X., Deng, H., Liu, H.: Thermodynamics for the adsorption of SO_2, NO and CO_2 from flue gas on activated carbon fiber. Chem. Eng. J. **200–202**, 399–404 (2012)
26. Fatemi, S., Vesali-Naseh, M., Cyrus, M., Hashemi, J.: Improving CO_2/CH_4 adsorptive selectivity of carbon nanotubes by functionalization with nitrogen-containing groups. Chem. Eng. Res. Des. **89**(9), 1669–1675 (2011)
27. Gui, M.M., Yap, Y.X., Chai, S.-P., Mohamed, A.R.: Multi-walled carbon nanotubes modified with (3-aminopropyl)triethoxysilane for effective carbon dioxide adsorption. Int. J. Greenhouse Gas Control **14**, 65–73 (2013)

28. Liu, Q., Shi, Y., Zheng, S., Ning, L., Ye, Q., Tao, M., He, Y.: Amine-functionalized low-cost industrial grade multi-walled carbon nanotubes for the capture of carbon dioxide. J. Energy Chem. **23**(1), 111–118 (2014)
29. Su, F., Lu, C., Chung, A.-J., Liao, C.-H.: CO_2 capture with amine-loaded carbon nanotubes via a dual-column temperature/vacuum swing adsorption. Appl. Energy **113**, 706–712 (2014)
30. Chan, K.C., Chao, C.Y.H., Wu, C.L.: Measurement of properties and performance prediction of the new MWCNT-embedded zeolite 13X/$CaCl_2$ composite adsorbents. Int. J. Heat Mass Transf. **89**, 308–319 (2015)
31. Chan, K.C.C., Christopher, Y.H.: Improved thermal conductivity of 13X/$CaCl_2$ composite adsorbent by cnt embedment. In: ASME Proceedings, Heat Transfer in EnergySystems, paper no, HT2013-17168, p. V001T01A040 (2013)
32. Han, T., Xiao, Y., Tong, M., Huang, H., Liu, D., Wang, L., Zhong, C.: Synthesis of CNT@MIL-68(Al) composites with improved adsorption capacity for phenol in aqueous solution. Chem. Eng. J. **275**, 134–141 (2015)
33. Xiang, Z., Hu, Z., Cao, D., Yang, W., Lu, J., Han, B., Wang, W.: Metal–organic frameworks with incorporated carbon nanotubes: improving carbon dioxide and methane storage capacities by lithium doping. Angew. Chem. Int. Ed. **50**(2), 491–494 (2011)
34. Anbia, M., Hoseini, V.: Development of MWCNT@MIL-101 hybrid composite with enhanced adsorption capacity for carbon dioxide. Chem. Eng. J. **191**, 326–330 (2012)
35. Biswas, P., Agrawal, S., Sinha, S.: Modeling and simulation for pressure swing adsorption system for hydrogen purification. Chem. Biochem. Eng. Q. **24**(4), 409–414 (2010)
36. Casas, N., Schell, J., Pini, R., Mazzotti, M.: Fixed bed adsorption of CO_2/H_2 mixtures on activated carbon: experiments and modeling. Adsorption **18**(2), 143–161 (2012)
37. Cavenati, S., Grande, C.A., Rodrigues, A.E.: Separation of mixtures by layered pressure swing adsorption for upgrade of natural gas. Chem. Eng. Sci. **61**(12), 3893–3906 (2006)
38. Chaffee, A.L., Knowles, G.P., Liang, Z., Zhang, J., Xiao, P., Webley, P.A.: CO_2 capture by adsorption: materials and process development. Int. J. Greenh. Gas Control **1**(1), 11–18 (2007)
39. Cho, S.-H., Park, J.-H., Beum, H.-T., Han, S.-S., Kim, J.-N.: A 2-stage PSA process for the recovery of CO_2 from flue gas and its power consumption*, in carbon dioxide utilization for global sustainability In: Proceedings of 7th international conference on carbon dioxide utilization. 2004, Elsevier BV. p. 405–410
40. Choi, W.-K., Kwon, T.-I., Yeo, Y.-K., Lee, H., Song, H.K., Na, B.-K.: Optimal operation of the pressure swing adsorption (PSA) process for CO_2 recovery. Korean J. Chem. Eng. **20**(4), 617–623 (2003)
41. Dantas, T.L., Amorim, S.M., Luna, F.M.T., Silva Jr., I.J., de Azevedo, D.C., Rodrigues, A.E., Moreira, R.F.: Adsorption of carbon dioxide onto activated carbon and nitrogen-enriched activated carbon: surface changes, equilibrium, and modeling of fixed-bed adsorption. Sep. Sci. Technol. **45**(1), 73–84 (2009)
42. Dantas, T.L.P., Luna, F.M.T., Silva, I.J., de Azevedo, D.C.S., Grande, C.A., Rodrigues, A.E., Moreira, R.F.P.M.: Carbon dioxide–nitrogen separation through adsorption on activated carbon in a fixed bed. Chem. Eng. J. **169**(1–3), 11–19 (2011)
43. Dantas, T.L.P., Luna, F.M.T., Silva, I.J., Torres, A.E.B., de Azevedo, D.C.S., Rodrigues, A.E., Moreira, R.F.P.M.: Carbon dioxide–nitrogen separation through pressure swing adsorption. Chem. Eng. J. **172**(2–3), 698–704 (2011)
44. Gomes, V.G., Yee, K.W.K.: Pressure swing adsorption for carbon dioxide sequestration from exhaust gases. Sep. Purif. Technol. **28**(2), 161–171 (2002)
45. Krishnamurthy, S., Rao, V.R., Guntuka, S., Sharratt, P., Haghpanah, R., Rajendran, A., Amanullah, M., Karimi, I.A., Farooq, S.: CO_2 capture from dry flue gas by vacuum swing adsorption: a pilot plant study. AIChE J. **60**(5), 1830–1842 (2014)
46. Lee, C.-H., Yang, J., Ahn, H.: Effects of carbon-to-zeolite ratio on layered bed H_2 PSA for coke oven gas. AIChE J. **45**(3), 535–545 (1999)
47. Park, J.-H., Kim, J.-N., Cho, S.-H.: Performance analysis of four-bed H_2 PSA process using layered beds. AIChE J. **46**(4), 790–802 (2000)
48. Wang, L., Liu, Z., Li, P., Yu, J., Rodrigues, A.E.: Experimental and modeling investigation on post-combustion carbon dioxide capture using zeolite 13X-APG by hybrid VTSA process. Chem. Eng. J. **197**, 151–161 (2012)
49. Wang, L., Yang, Y., Shen, W., Kong, X., Li, P., Yu, J., Rodrigues, A.E.: Experimental evaluation of adsorption technology for CO_2 capture from flue gas in an existing coal-fired power plant. Chem. Eng. Sci. **101**, 615–619 (2013)
50. Britt, D., Furukawa, H., Wang, B., Glover, T.G., Yaghi, O.M.: Highly efficient separation of carbon dioxide by a metal-organic framework replete with open metal sites. Proc. Natl. Acad. Sci. **106**(49), 20637–20640 (2009)
51. Qadir, N.U., Said, S.A.M., Mansour, R.B., Mezghani, K., Ul-Hamid, A.: Synthesis, characterization, and water adsorption properties of a novel multi-walled carbon nanotube/MIL-100(Fe) composite. Dalton Trans. **45**(39), 15621–15633 (2016)
52. Wang, L.J., Deng, H., Furukawa, H., Gándara, F., Cordova, K.E., Peri, D., Yaghi, O.M.: Synthesis and characterization of metal-organic framework-74 containing 2, 4, 6, 8, and 10 different metals. Inorg. Chem. **53**(12), 5881–5883 (2014)
53. Seo, Y.-K., Yoon, J.W., Lee, J.S., Lee, U.H., Hwang, Y.K., Jun, C.-H., Horcajada, P., Serre, C., Chang, J.-S.: Large scale fluorine-free synthesis of hierarchically porous iron(III) trimesate MIL-100(Fe) with a zeolite MTN topology. Microporous Mesoporous Mater. **157**, 137–145 (2012)
54. Rouquerol F, Rouquerol J, Sing K.: Adsorption by Powders and Porous Solids: Principles, Methodology and Application. Academic Press, London (1999)
55. Simmons, J.M., Wu, H., Zhou, W., Yildirim, T.: Carbon capture in metal–organic frameworks—a comparative study. Energy Environ. Sci. **4**(6), 2177–2185 (2011)
56. Mei, L., Jiang, T., Zhou, X., Li, Y., Wang, H., Li, Z.: A novel DOBDC-functionalized MIL-100(Fe) and its enhanced CO_2 capacity and selectivity. Chem. Eng. J. **321**, 600–607 (2017)
57. Ben-Mansour, R., Basha, M., Qasem, N.A.A.: Multicomponent and multi-dimensional modeling and simulation of adsorption-based carbon dioxide separation. Comput. Chem. Eng. **99**(Supplement C), 255–270 (2017)
58. Ben-Mansour, R., Qasem, N.A.A.: An efficient temperature swing adsorption (TSA) process for separating CO_2 from CO_2/N_2 mixture using Mg-MOF-74. Energy Convers. Manage. **156**(Supplement C), 10–24 (2018)
59. Qasem, N.A.A., Ben-Mansour, R.: Energy and productivity efficient vacuum pressure swing adsorption process to separate CO_2 from CO_2/N_2 mixture using Mg-MOF-74: a CFD simulation. Appl. Energy **209**(Supplement C), 190–202 (2018)
60. Klinkenberg, A.: Heat transfer in cross-flow heat exchangers and packed beds. Ind. Eng. Chem. **46**(11), 2285–2289 (1954)
61. Luciano, R.S.: Structured zeolite adsorbents for CO_2 separation. 2012, MS thesis, Luleå University of Technology, Luleå, Sweden
62. Han, Z., Fina, A.: Thermal conductivity of carbon nanotubes and their polymer nanocomposites: a review. Prog. Polym. Sci. **36**(7), 914–944 (2011)
63. Munusamy, K., Sethia, G., Patil, D.V., Somayajulu Rallapalli, P.B., Somani, R.S., Bajaj, H.C.: Sorption of carbon dioxide, methane, nitrogen and carbon monoxide on MIL-101(Cr): volumetric measurements and dynamic adsorption studies. Chem. Eng. J. **195–196**, 359–368 (2012)

64. Qasem, N.A.A., Ben-Mansour, R., Habib, M.A.: Enhancement of adsorption carbon capture capacity of 13X with optimal incorporation of carbon nanotubes. Int. J. Energy Environ. Eng. **8**(3), 219–230 (2017)